Inorg. Chem. **2003**, *42*, 6412–6424

$REMGa_3Ge$ and $RE_3Ni_3Ga_8Ge_3$ (M = Ni, Co; RE = Rare-Earth Element): New Intermetallics Synthesized in Liquid Gallium. X-ray, Electron, and Neutron Structure Determination and Magnetism

Marina A. Zhuravleva,[†] Robert J. Pcionek,[†] Xiaoping Wang,[‡] Arthur J. Schultz,[‡] and Mercouri G. Kanatzidis*,[†]

Department of Chemistry, Michigan State University, East Lansing, Michigan 48824, and Intense Pulsed Neutron Source, Argonne National Laboratory, Argonne, Illinois 60439

Received February 19, 2003

New quaternary intermetallic phases $REMGa_3Ge$ (**1**) (RE = Y, Sm, Tb, Gd, Er, Tm; M = Ni, Co) and $RE_3Ni_3Ga_8Ge_3$ (**2**) (RE = Sm, Gd) were obtained from exploratory reactions involving rare-earth elements (RE), transition metal (M), Ge, and excess liquid Ga the reactive solvent. The crystal structures were solved with single-crystal X-ray and electron diffraction. The crystals of **1** and **2** are tetragonal. Single-crystal X-ray data: $YNiGa_3Ge$, $a = 4.1748(10)$ Å, $c = 23.710(8)$ Å, $V = 413.24(2)$ Å^3, $I4/mmm$, $Z = 4$; $Gd_3Ni_3Ga_8Ge_3$, $a = 4.1809(18)$ Å, $c = 17.035(11)$ Å, $V = 297.8(3)$ Å^3, $P4/mmm$, $Z = 1$. Both compounds feature square nets of Ga atoms. The distribution of Ga and Ge atoms in the $REMGa_3Ge$ was determined with neutron diffraction. The neutron experiments revealed that in **1** the Ge atoms are specifically located at the 4*e* crystallographic site, while Ga atoms are at 4*d* and 8*g*. The crystal structures of these compounds are related and could be derived from the consecutive stacking of disordered $[MGa]_2$ puckered layers, monatomic RE–Ge planes and $[MGa_4Ge_2]$ slabs. Complex superstructures with modulations occurring in the *ab*-plane and believed to be associated with the square nets of Ga atoms were found by electron diffraction. The magnetic measurements show antiferromagnetic ordering of the moments located on the RE atoms at low temperature, and Curie–Weiss behavior at higher temperatures with the values of μ_{eff} close to those expected for RE^{3+} free ions.

Introduction

The application of molten aluminum as a reactive solvent for the exploratory synthesis of complex intermetallic compounds led to the discovery of a number of new multinary phases including $Sm_2Ni(Ni_xSi_{1-x})Al_4Si_6$,[1] $Ln_2Al_3Si_2$,[2] $RENiAl_4Ge_2$,[3] $RE_8Ru_{12}Al_{49}Si_9(Al_xSi_{12-x})$,[4] $Tb_2NiAl_4Ge_2$, and $Ce_2NiAl_{6-x}Ge_{4-y}$.[5] Following these promising results, we became interested in the reactivity and phase formation in the related systems RE/M/Ga/Ge, where RE = rare-earth metal and M = Ni and Co, for reactions conducted in liquid Ga. From these studies, we have recently reported the hexagonal compounds $RE_{0.67}M_2Ga_{5-x}Tt_x$ and $RE_{0.67}M_2Ga_{6-x}Tt_x$[6] (Tt = Si or Ge) that are very stable and readily form at the ratio RE:M < 1 within a rather broad range of synthetic conditions. However, when we turn to the compositions with RE:M ≥ 1, we find that the reaction product strongly depends on RE and is also significantly more sensitive to the reaction conditions. Specifically, the hexagonal phases do not form; instead, we obtain the tetragonal $REMGa_3Ge$, $RE_2MGa_9Ge_2$,[7]

* To whom correspondence should be addressed. E-mail: kanatzid@cem.msu.edu.
[†] Michigan State University.
[‡] Argonne National Laboratory.

(1) Chen, X. Z.; Sportouch, S.; Brazis, P.; Kannewurf, C. R.; Cowen, J. A.; Patschke, R.; Kanatzidis, M. G. *Chem. Mater.* **1998**, *10*, 3202.
(2) Chen, X. Z.; Sieve, B.; Henning, R.; Schultz, A. J.; Brazis, P.; Kannewurf, C. R.; Cowen, J. A.; Crosby, R.; Kanatzidis, M. G. *Angew. Chem., Int. Ed.* **1999**, *38*, 693.
(3) (a) Sieve, B.; Chen, X. Z.; Cowen, J. A.; Larson, P.; Mahanti. S. D.; Kanatzidis, M. G. *Chem. Mater.* **1999**, *11*, 2451. (b) Wu, X.; Latturner, S.; Kanatzidis, M. G. Work in progress.
(4) Sieve, B.; Chen, X. Z.; Henning, R.; Brazis, P.; Kannewurf, C. R.; Cowen, J. A.; Schultz, A. J.; Kanatzidis, M. G. *J. Am. Chem. Soc.* **2001**, *29*, 7040.
(5) Sieve, B.; Trikalitis, P. N.; Kanatzidis, M. G. *Z. Anorg. Allg. Chem.* **2002**, *628*, 1568.
(6) Zhuravleva, M. A.; Chen, X. Z.; Wang, X.; Schultz A. J.; Ireland, J.; Kannewurf, C. R.; Kanatzidis, M. G. *Chem. Mater.* **2002**, *14* (7), 3066.
(7) Zhuravleva, M. A. Doctoral Dissertation Thesis, Michigan State University, 2003.

10.1021/ic0341892 CCC: $25.00
Published on Web 09/12/2003

$RE_3Ni_3Ga_8Ge_3$, and the orthorhombic $RE_4Ni_3Ga_6Ge_4$[7] phases. The results are reminiscent of those obtained in the corresponding RE/Ni/Al/Si and RE/Ni/Ga/Si systems, in which the orthorhombic/tetragonal compounds $Sm_2Ni(Ni_xSi_{1-x})Al_4Si_6$[1] and $RE_2NiGa_{12-x}Si_x$[8] were produced at Sm:Ni > 1. Here we report the synthesis, crystal structure, and magnetic properties of two new families of quaternary intermetallic compounds $REMGa_3Ge$ (RE = Y, Sm, Tb, Gd, Er, Tm; M = Ni, Co) and $RE_3Ni_3Ga_8Ge_3$ (RE = Sm, Gd) grown from Ga flux. We also address the issue of Ga/Ge distribution and the question of disorder versus long-range ordering using neutron diffraction and electron diffraction, respectively.

Experimental Section

Synthesis. The reactions between the rare-earth element, transition metal (Ni or Co), and Ge were performed in liquid Ga. Elemental rare earths (Y, Sm, Gd, Tb, Er, Tm) typically of purity 99.9% and higher (CERAC Inc.), nickel (cobalt) powder 99.99% (Aldrich Inc.), Ge powder (99.999%, CERAC Inc.), and Ga (3 mm shots 99.999%, CERAC Inc.) were taken in the amounts RE 0.75 mmol, Ni 0.75 mmol, Ga 11.2 mmol, and Ge 0.75 mmol and loaded into alumina crucibles under an inert (N_2) atmosphere. The crucibles were placed into fused silica tubes and evacuated ($\sim 1 \times 10^{-4}$ Torr). The following heat treatment was used: the temperature was raised to 1000 °C at the rate 60 °C/h and kept at 1000 °C for 5 h to achieve proper melt, then cooled to 850 °C in 2 h and kept isothermally at 850 °C for 36 h and, finally, slowly cooled to 250 °C at the rate 33 °C/h. The majority of the unused flux was next removed by centrifuging liquid Ga through a coarse frit at ~250 °C. The reaction products were further isolated from the remaining Ga by soaking in a ~5 M solution of iodine in dimethylformamide (DMF) over 12 h at room temperature. This step serves to dissolve the residual Ga by converting it to GaI_3. The resulting crystalline product was subsequently rinsed with DMF and dried with acetone and ether. The phases **1** and **2** were recovered in high yields (80−95%) from the reactions in molten Ga. The isolated crystals possessed a typical platelike morphology, often with a phyllomorphic character. Images of characteristic crystals of **1** and **2** are shown in the SEM micrographs in Figure 1A and Figure 1B.

X-ray Powder Diffraction. The X-ray diffraction (XRD) powder patterns of products were taken at room temperature on a Rigaku-Denki/Rw400F2 (rotaflex) rotating-anode (Cu Kα) powder diffractometer and a CPS 120 INEL X-ray diffractometer (Cu Kα) equipped with a position-sensitive detector. Experimental powder patterns were compared to that calculated from single-crystal data using the CERIUS^2 software package.[9]

RE/Ni/Ga/Ge (RE = Y, Sm, Gd, and Tb) Phase Composition. The examination of the powder patterns immediately revealed the differences in the reaction products depending on the type of the RE used. Hence, when RE = Y, Tb, Er, or Tm, the peaks in the XRD pattern showed single-phase $RENiGa_3Ge$ (**1**), while for RE = Gd the patterns indicated ~80% of compound $Gd_3Ni_3Ga_8Ge_3$ (**2**) with impurities that included hexagonal $Gd_{0.67}Ni_2Ga_{6-x}Ge_x$ and Ge. In the case of Sm, up to three quaternary phases $SmNiGa_3Ge$, $Sm_2NiGa_9Ge_2$, and $Sm_3Ni_3Ga_8Ge_3$ could be found in the reaction product.

RE/Co/Ga/Ge (RE = Y, Sm, Gd, and Er) Phase Composition. For the Co-containing reactions with Y, Gd, and Sm the yield of quaternary phases of type **1** is very high. The minor side products (~5%) for these reactions were $CoGa_3$ and Ge. In the case of Er, the quaternary phase **1** did not form; instead a single phase of $ErCoGa_5$ ($HoCoGa_5$ structure type[10]) was produced.

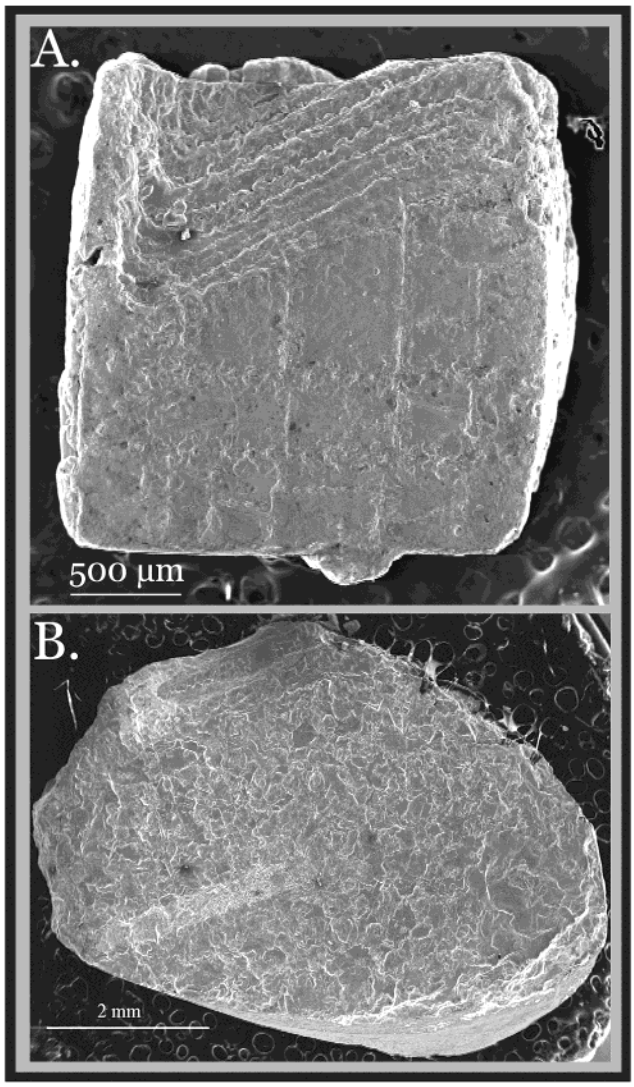

Figure 1. The SEM photographs of crystals of (A) $GdCoGa_3Ge$ (**1**) and (B) $Sm_3Ni_3Ga_8Ge_3$ (**2**) grown from liquid Ga at 850 °C. The roughening of the surface of the crystals is most likely due to the etching effect of I_2 during isolation.

Elemental Analysis. The chemical composition of the products was determined by energy dispersive spectroscopy (EDS) performed on a JEOL JSM-35C scanning electron microscope (SEM) equipped with a NORAN Inc. EDS detector. The analysis was conducted at accelerating voltage 20 kV and collection time 30 s. After averaging the results of the elemental analysis over several crystals of each analogue, the compositions of compounds **1** and **2** were determined to be "$RE_{1.1}MGa_3Ge_{1.1}$" and "$RE_3Ni_{2.3}Ga_8Ge_{2.5}$", respectively. The formulas for **1** and **2** obtained from the elemental analysis agreed well with those refined from the single-crystal data.

Single-Crystal X-ray Diffraction. Intensity data were collected on single crystals of **1** ($YNiGa_3Ge$) and **2** ($Gd_3Ni_3Ga_8Ge_3$) at room temperature with a Siemens Platform SMART[11] CCD X-ray

(8) Chen, X. Z.; Small, P.; Sportouch, S.; Zhuravleva, M.; Brazis, P.; Kannewurf, C. R.; Kanatzidis, M. G. *Chem. Mater*. **2000**, *12*, 2520.
(9) *CERIUS^2, version 1.6*; Molecular Simulations Inc.: Cambridge, England, 1994.
(10) Grin', Yu. N.; Yarmolyuk, Ya. P.; Gladyshevskii, E. I. *Sov. Phys. Crystallogr*. (translated from *Kristallografiya*) **1979**, *24* (2), 137.
(11) *SMART, version 5*; Siemens Analytical X-ray Systems, Inc.: Madison, WI, 1998.

Table 1. X-ray Single Crystal Data and Structure Refinement for $YNiGa_3Ge$ (**1**) and $Gd_3Ni_3Ga_8Ge_3$ (**2**)

empirical formula	$YNiGa_3Ge$	$Gd_3Ni_{2.79}Ga_8Ge_3$
fw	429.37	1411.08
crystal system	tetragonal	tetragonal
space group	*I*4/*mmm* (No. 139)	*P*4/*mmm* (No. 123)
unit cell dimens (Å) (at 296 K)	$a = 4.1748(10)$ $c = 23.710(8)$	$a = 4.1809(18)$ $c = 17.035(11)$
volume (Å^3), *Z*	413.24(19), 4	297.8(3), 4
density (calcd) (g/cm^3)	6.901	7.869
absorption coeff (mm^{-1})	44.575	45.870
reflections collected	1944	3830
independent reflections	194 [R(int) = 0.0569]	391 [$R_{int} = 0.0850$]
data/parameters	194/22	391/35
final R indices [$I > 2\sigma(I)$][a]	R1 = 0.0298, wR2 = 0.0787[b]	R1 = 0.0360, wR2 = 0.0889[c]
R indices (all data)	R1 = 0.0333, wR2 = 0.0797	R1 = 0.0414, wR2 = 0.0909
largest diff peak and hole (e/Å^3)	0.987 and −1.460	2.744 and −4.546

[a] $R1 = \sum||F_o| - |F_c||/\sum|F_o|$; $wR2 = [w\{|F_o| - |F_c|\}^2/w|F_o|^2]^{1/2}$. [b] $w = 1/[\sigma^2(F_o^2) + (0.0451P)^2]$; where $P = (1/3)F_o^2 + (2/3)F_c^2$. [c] $w = 1/[\sigma^2(F_o^2) + (0.0575P)^2]$; where $P = (1/3)F_o^2 + (2/3)F_c^2$.

diffractometer. Crystals of suitable size 0.08 × 0.12 × 0.01 mm^3 and 0.07 × 0.06 × 0.02 mm^3 were cut out of larger crystals and mounted on glass fibers. Both data sets (Mo Kα radiation, λ = 0.71073 Å) were acquired up to 66.5° in 2θ, covering either a full sphere or a hemisphere of reciprocal space. The individual frames were measured using the ω-steps of 0.30° and exposure time up to 60 s per frame. The data reduction was performed with the SAINTPLUS[12] software package. A face-indexing procedure was used for analytical absorption corrections. An additional correction for absorption based on symmetry equivalent reflections was subsequently applied with the SADABS program. The structure solution and refinement were done by direct methods with the SHELXTL software package. All atomic positions were refined anisotropically. The setting of the cell was standardized with STRUCTURE TIDY program.[13] The information relevant to the data collection and structure refinement is given in Table 1. The complete crystallographic information can be obtained in the Supporting Information section.

$YNiGa_3Ge$ (**1**) crystallizes in the tetragonal space group *I*4/*mmm*. The asymmetric unit of $YNiGa_3Ge$ contains a total of seven atomic positions. The Y atoms reside at 4*e* positions, the Ga atoms occupy 8*g* and 4*d* sites, and Ni atoms are found at 2*a* and 4*e* sites. The Ge was refined as a split position with 50% occupancy on each of the Ge(1) and Ge(2) sites. The refinement of Ge in a single 4*e* site resulted in the enlarged thermal displacement parameter (U_{eq} up to ~100 Å^2 × 10^{-3}) and increased R values (17% and higher). The partial occupancy of 50% was also refined for the Ni at 4*e*, as a result of the close interatomic distances to one of the split positions of Ge. The disorder observed for Ni(2) and Ge(2) also affects the Ga(2) square net lying right beneath. For this reason, the enlarged thermal displacement parameters were found for Ga(2), even though these atoms are ordered. The final atomic positions, the equivalent thermal displacement parameters, and occupancies are listed in Table 2; the interatomic distances up to 3.5 Å are presented in Table 3.

The $RE_3Ni_3Ga_8Ge_3$ (**2**) are structurally related to the $REMGa_3Ge$, and they crystallize in the tetragonal space group *P*4/*mmm*. Owing to this symmetry reduction, an increased number of atomic positions (a total of 10) were identified in the structure of $Gd_3Ni_3Ga_8Ge_3$.

Table 2. Atomic Coordinates, Equivalent Isotropic Displacement Parameters (Å^2 × 10^3), and Occupancies for $YNiGa_3Ge$ (**1**)

atom	Wyckoff symbol	*x*	*y*	*z*	U_{eq}[a]	occ
Y(1)	4e	0	0	0.1496(1)	8(1)	1
Ga(1)	8g	0	1/2	0.0551(1)	14(1)	1
Ga(2)	4d	0	1/2	1/4	31(1)	1
Ni(1)	2a	0	0	0	9(1)	1
Ni(2)	4e	0	0	0.2831(2)	19(1)	1/2
Ge(1)	4e	0	0	0.3523(2)	13(1)	1/2
Ge(2)	4e	0	0	0.3794(2)	13(1)	1/2

[a] U_{eq} is defined as one-third of the trace of the orthogonalized $\mathbf{U}_{ij}$ tensor.

Table 3. Selected Bond Lengths (Å) for $YNiGa_3Ge$ (**1**)

bond	distance	mult	bond	distance	mult
Y(1)−Ge(1)	2.9524(7)	×4	Ga(2)−Ga(2)	2.9520(7)	×4
Y(1)−Ge(2)	3.0316(13)	×4	Ge(1)−Ge(2)	0.645(4)	×1
Y(1)−Ga(1)	3.0622(14)	×4	Ge(1)−Ni(2)	1.640(6)	×1
Y(1)−Ga(2)	3.1652(12)	×4	Ge(2)−Ga(1)	2.600(3)	×4
Y(1)−Ni(2)	3.355(2)	×4	Ga(1)−Ni(1)	2.4631(8)	×2
Ni(1)−Ga(1)	2.4632(8)	×8	Ga(1)−Ga(1)	2.615(3)	×1
Ni(2)−Ga(2)	2.2298(15)	×3	Ga(1)−Ga(1)	2.9520(7)	×4
Ni(2)−Ge(2)	2.285(6)	×1			

Table 4. Atomic Coordinates, Equivalent Isotropic Displacement Parameters (Å^2 × 10^3), and Occupancies for $Gd_3Ni_3Ga_8Ge_3$ (**2**)

position	Wyckoff symbol	*x*	*y*	*z*	U_{eq}[a]	occ
Gd(1)	1a	0	0	0	9(1)	1
Gd(2)	2h	1/2	1/2	0.2862(1)	9(1)	1
Ge(1)	1c	1/2	1/2	0	98(4)	1
Ge(2)	2g	0	0	0.3307(2)	8(1)	0.59(3)
Ge(2′)	2g	0	0	0.2939(6)	17(1)	0.40(4)
Ga(1)	4i	0	1/2	0.4233(1)	13(1)	1
Ga(2)	4i	0	1/2	0.1401(1)	23(1)	1
Ni(1)	1d	1/2	1/2	1/2	10(1)	1
Ni(2)	2g	0	0	0.1959(2)	11(1)	0.714(14)
Ni(2′)	2h	1/2	1/2	0.0997(4)	10(1)	0.223(14)

[a] U_{eq} is defined as one-third of the trace of the orthogonalized $\mathbf{U}_{ij}$ tensor.

Thus, the Gd atoms in the asymmetric unit of **2** occupy two atomic sites (1*a* and 2*h*), and the number of sites occupied by Ni and Ge increased to three (1*d*, 2*g*, 2*h* and 1*c*, 2*g*, 2*g*, respectively). The Ga atoms are found in two positions with multiplicity 4*i*. Similar to $REMGa_3Ge$ disorder is observed in the structure of $Gd_3Ni_3Ga_8Ge_3$ causing the short bond distances between Ni and Ge. Partial occupancies of 0.714(14) and 0.223(14) were found for the disordered atoms Ni(2) and Ni(2′), respectively. The occupancies of the Ge(2)/Ge(2′) split site refined to 0.59(4)/0.40(3), while the Ge(1) site, although exhibiting an enlarged thermal displacement parameter, refined to full occupancy and did not favor the split position during the refinement. The final atomic positions, the equivalent thermal displacement parameters, and occupancies for **2** are presented in Table 4. The interatomic distances up to 3.5 Å are listed in Table 5.

The apparent disorder observed in these two structures is evidently pointing to a possible supercell. However, no clear indication of it could be seen from the X-ray data except for the $RECoGa_3Ge$ (RE = Y, Sm, Gd), where the reciprocal lattice featured satellite reflections with incommensurate spacings. We observed that the supercell reflections are generally too weak to be accurately measured. To further probe the longer range ordering, we performed electron diffraction studies (see below).

Because the X-ray scattering power of Ga and Ge is nearly identical, elemental analysis was used in combination with bond

(12) *SAINT*, *version 4*; Siemens Analytical X-ray Systems, Inc.: Madison, WI, 1994−1996.
(13) Gelato, L. M.; Parthé, E. *J. Appl. Crystallogr*. **1987**, *20*, 139.

Table 5. Selected Bond Lengths (Å) for $Gd_3Ni_3Ga_8Ge_3$ (**2**)

bond	distance	mult	bond	distance	mult
Gd(1)−Ge(1)	2.9563(13)	×4	Ge(2′)−Ni(2)	1.670(11)	×1
Gd(2)−Ge(2′)	2.9593(14)	×4	Ge(1)−Ni(2′)	1.699(7)	×2
Gd(2)−Ge(2)	3.0522(14)	×4	Ge(2)−Ni(2)	2.297(5)	×1
Gd(2)−Ga(1)	3.1344(16)	×4	Ge(2)−Ga(1)	2.618(2)	×4
Gd(1)−Ga(2)	3.1722(16)	×8	Ga(1)−Ni(1)	2.4653(11)	×2
Gd(2)−Ga(2)	3.2508(17)	×1	Ga(1)−Ga(1)	2.9563(13)	×4
Gd(2)−Ni(2)	3.3325(18)	×3	Ga(2)−Ni(2′)	2.200(2)	×2
Gd(1)−Ni(2′)	3.410(4)	×3	Ga(2)−Ni(2)	2.2967(16)	×2
Ge(2)−Ge(2′)	0.628(8)	×1	Ga(2)−Ga(2)	2.9563(13)	×4

distance considerations to assign the Ga and Ge atoms positions. However, in order to accurately determine these positions, neutron diffraction was used. The neutron scattering power between Ga and Ge differs by ∼10% compare to ∼3% for the X-ray radiation.

Single-Crystal Neutron Structure Determination of 1. Neutron diffraction data were collected from a single crystal of $YCoGa_3Ge$ (**1**) at the Intense Pulsed Neutron Source (IPNS), Argonne National Laboratory. The single-crystal diffractometer (SCD) is a time-of-flight instrument with a time- and position-sensitive detector. A detailed description of the SCD instrument and data collection and analysis procedures have been published.[14,15] A total of 13 histograms were measured at χ and ϕ values suitable to cover a unique octant of reciprocal space. An auto-indexing algorithm[16] was used to obtain an initial orientation matrix from the peaks in one histogram. Data were indexed using individual orientation matrices for each histogram to allow for any misalignment of the sample. Bragg peaks were integrated in three dimensions about their predicted locations and corrected for the incident neutron spectrum and detector efficiency. The lattice constants were refined using 299 intense peaks, corresponding to an *I*-centered tetragonal cell with $a = 4.1882(7)$ Å and $c = 23.776(9)$ Å. The intensities were corrected for absorption using a local program ANVRED and assuming a spherical crystal of radius 1.27 mm, and wavelength-dependent linear absorption coefficients of $\mu(\text{cm}^{-1}) = 0.409 + 0.262\lambda$. The GSAS software package[17] was used for structural analysis. The refinement was based on *F* using reflections with $|F_o| > 3\sigma(F_o)$. Initial coordinates were obtained from single-crystal X-ray analysis. The information relative to neutron data collection and refinement of **1** is given in Table 6; the positional and thermal displacement parameters and occupancies are presented in Table 7. The selected interatomic distances are listed in Table 8.

Refinement of the neutron structure shows that our original X-ray assignment of Ga and Ge atoms (based on bond distances) was correct, i.e., the Ge atoms indeed occupy 4*e* sites, while Ga was refined on the 8*g* and 4*d* sites. The neutron refinement also confirmed that the Ge atoms in **1** are in split sites with 50% occupancy on each, and the Co 4*e* position is 50% occupied. Thus, the unit cell composition of **1** can be formulated as $YCoGa_3Ge$ with $Z = 4$.

Transmission Electron Microscopy and Electron Diffraction. The transmission electron microscopy (TEM) studies were performed on a JEOL 100CX TEM microscope. The electron beam was generated from the CeB_6 filament at accelerating voltage 120 kV. Both the imaging mode and the selected area electron diffraction (SAED) mode were used. The samples were stable under the impact of the electron beam.

Table 6. Neutron Crystal Data and Structural Refinement Parameters for $YCoGa_3Ge$ (**1**)

formula	$YCoGa_3Ge$
fw	429.62
temperature, K	295
crystal system	tetragonal
space group	*I*4/*mmm*
a, Å	4.1882(7)
c, Å	23.7760(9)
V, Å^3	417.1(2)
Z	4
d_{calcd}, g/cm^3	6.84
radiation	neutrons
data collection technique	time-of-flight Laue
$\mu(\lambda)$, cm^{-1}	$0.409 + 0.262\lambda$
reflns ($I > 3\sigma(I)$)/parameters	433/34
refinement method	full-matrix least-squares on *F*
R indices $R_w(F)$,[a] $R(F)$[b]	0.062, 0.068

[a] $R_w(F) = \{\sum[w(F_o - F_c)^2]/\sum[w(F_o)^2]\}^{1/2}$. [b] $R(F) = \sum[|F_o| - |F_c|]/\sum|F_o|$.

Table 7. Fractional Coordinates and Site Occupancy of $YCoGa_3Ge$ (**1**)

position	Wyckoff symbol	*x*	*y*	*z*	occ
Y	4e	0	0	0.14900(7)	1
Ga(1)	8g	0	1/2	0.05446(6)	1
Ga(2)	4d	0	1/2	1/2	1
Co(1)	2a	0	0	0	1
Co(2)	4e	0	0	0.2777(5)	1/2
Ge(1)	4e	0	0	0.3562(3)	1/2
Ge(2)	4e	0	0	0.3754(2)	1/2

Table 8. Selected Interatomic Distances (Å) for $YCoGa_3Ge$ (**1**)

bond	distance	bond	distance
Y−Ge(1)	2.9641(6)	Co(2)−Ga(2)	2.195(4)
Y−Ge(2)	3.018(1)	Co(2)−Ge(2)	2.323(13)
Y−Co(2)	3.060(12)	Ga(1)−Ga(1)	2.590(3)
Y−Ga(2)	3.186(1)	Ga(1)−Ga(1)	2.9615(5)
Y−Ga(1)	3.072(2)	Ga(1)−Ge(1)	2.982(5)
Y−Co(2)	3.436(6)	Ga(1)−Ge(2)	2.677(3)
Co(1)−Ga(1)	2.462(1)		

Sample Preparation for TEM. Large, often square platelike single crystals of **1** and irregularly shaped flat single crystals of **2**, normally over 10 mm^2 in area and up to 600 μm in thickness, were selected. The samples were hand-polished with subsequently increasing grit (1000−1500) sandpaper to approximately 200−300 μm in thickness. A core drill was then used to cut out circular-shaped specimens 3 mm in diameter, suitable for use in the TEM holder. As-prepared samples were electrolytically thinned using a Tenupole-3 twin-jet polishing unit equipped with an infrared detector. The electropolishing experiment was conducted in the temperature range from −35 to −40 °C with a 15 V applied potential using a four-component acidic electrolyte.[18] The mean size of the resultant hole is regularly ∼100 μm in diameter, with the average area lucent to the electron beam on the order of 400 μm^2. Due to the platelike habit of the crystals, in most cases the [001] zone axis could be observed at zero tilt. It is only in the case of $GdCoGa_3Ge$ that it was possible to observe the transverse [010] zone axis owing to the unusual cuboid shape of the crystal.

Magnetic Measurements. The magnetic susceptibility was measured on single crystal and polycrystalline samples of **1** ($TbNiGa_3Ge$, $GdCoGa_3Ge$, and $YCoGa_3Ge$) and **2** ($Gd_3Ni_3Ga_8Ge_3$) as a function of temperature in the range 2−400 K in an applied external magnetic field of 500 G with MPMS Quantum Design

(14) Schultz, A. J.; Van Derveer, D. G.; Parker, D. W.; Baldwin, J. E. *Acta Crystallogr., Sect. C* **1990**, *C46*, 276.
(15) Schultz, A. J. *Trans. Am. Crystallogr. Assoc.* **1987**, *23*, 61.
(16) Jacobson, R. A. *J. Appl. Crystallogr.* **1986**, *19*, 283.
(17) Larson, A. C.; Von Dreele R. B. *GSAS General Structural Analysis System*; Los Alamos National Laboratory: Los Alamos, NM, 2000.

(18) Electrolyte composition (vol %): 10% H_2SO_4, 1% HF, 1.5% H_2NO_3, 87.5% CH_3OH.

Inc. SQUID magnetometer. The field dependence of the magnetic susceptibility was determined at 2−3 K in the fields up to ±5 T. The susceptibility data was corrected for the sample holder contribution. The isotropic measurements ($TbNiGa_3Ge$, $GdCoGa_3Ge$, and $YCoGa_3Ge$) were carried out using ground polycrystalline samples. For anisotropic measurements ($GdCoGa_3Ge$ and $Gd_3Ni_3Ga_8Ge_3$) crystals with explicit platelike morphology were placed with the *c*-axis parallel and perpendicular to the external magnetic field.

Results and Discussion

Reaction Chemistry. The reaction chemistry in the system RE/M/Ga/Ge (RE = rare-earth, M = Ni, Co) conducted in excess Ga with RE:M ≥ 1 is one of the most complex among metal flux systems. For example, in previous studies in the related systems with Al (RE/M/Al/Ge, RE/M/Al/Si) and with Ga (RE/M/Ga/Si and RE/M/Ga/Ge with RE:M < 1) we observed that, generally, for a given set of reaction conditions, a series of isotypic compounds with different RE and/or M metal could be obtained. For instance, over 20 analogues of $RE_{0.67}M_2Ga_{5-x}Tt_x$[6,7] and $RE_{0.67}M_2Al_{5-x}Tt_x$[19] (Tt = Si or Ge) have been obtained and nearly every heavy RE analogue of $RENiAl_4Ge_2$[3] grown. For the first time in the RE/M/Ga/Ge system, with RE:M ≥ 1, we observe a delicate sensitivity of the products to the reaction conditions and a large variation of the crystal structure with the RE element.

Thus, for M = Ni the reaction of different lanthanide elements under otherwise identical conditions results in $YNiGa_3Ge$, $Ce_2NiGa_9Ge_2$,[7] $Gd_3Ni_3Ga_8Ge_3$, and $TbNiGa_3Ge$. The case is even more complicated for Sm, as up to three phases $Sm_2NiGa_9Ge_2$,[7] $SmNiGa_3Ge$, and $Sm_3Ni_3Ga_8Ge_3$ could be found in the reaction product. The latter two possibly form an intergrowth in one isolated crystal. Furthermore, increased reaction times (3−6 days) with Tb and Y produced $Y_4Ni_3Ga_6Ge_4$ and $Tb_4Ni_3Ga_6Ge_4$[7] (compared to $YNiGa_3Ge$ and $TbNiGa_3Ge$ obtained in shorter reaction times). Interestingly, if Ni is substituted for Co, the following phases form in quantitative yield: $YCoGa_3Ge$, $Ce_2CoGa_9Ge_2$,[7] $SmCoGa_3Ge$, $GdCoGa_3Ge$, and $ErCoGa_5$[10] for RE = Y, Ce, Sm, Gd, and Er, respectively. As we will describe below, these different phases share many structural components and may have similar formation energies. Also, some may be intermediates that have been quenched before had a chance to transform to the more thermodynamically stable ones.

Crystal Structure of 1. The crystal structure of $REMGa_3Ge$ derives from the Ce_2NiGa_{10} structure type;[20] however, no disorder has been reported for the latter. To show the relationship of these two structures, we can rewrite the formula of the Ce_2NiGa_{10}-type and **1** as $RE_4Ni_2[Ga'_4Ga''_{12}Ga'''_4]$ and $RE_4M_2[M_2\square_2Ga''_{12}Ge_4]$, respectively. In this formulation the different crystal sites in their structures are clearly indicated. Thus, the relation of **1** to Ce_2NiGa_{10} lies in substitution of Ga′ with M and a vacancy (□), plus a substitution of Ga‴ with Ge. The $REMGa_3Ge$ compounds

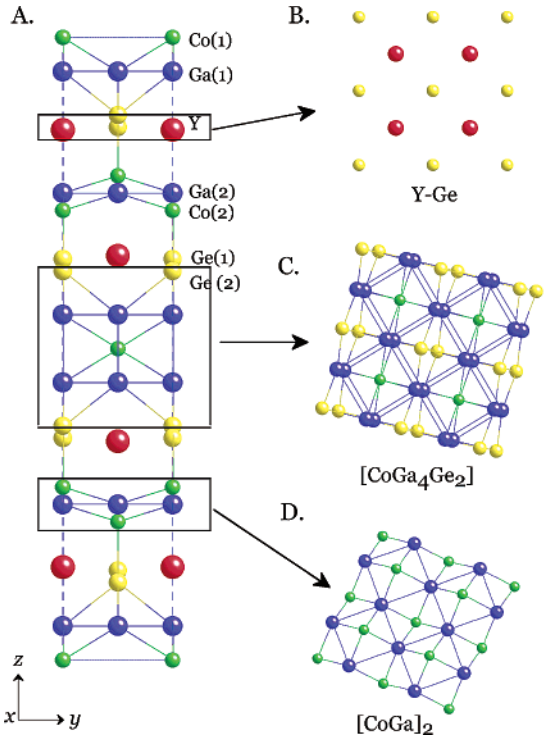

Figure 2. The structure of $YCoGa_3Ge$ (**1**): (A) a single unit cell viewed along the *b*-axis; (B) the Y−Ge monatomic layer projected onto the *ab*-plane; (C) the $[CoGa_4Ge_2]$ slab viewed approximately along the *c*-axis; (D) the $[CoGa]_2$ puckered layer.

are the first gallium-containing analogues in this structure type. The quaternary aluminum isotype $Ce_2NiAl_{6-x}Ge_{4+y}$ has been recently reported.[5] The crystal structure of the $YCoGa_3Ge$, as refined using neutron diffraction data and projected onto the *bc*-plane, is depicted in Figure 2A. In this plot, no bonds were drawn to the Y atoms in order to emphasize the different types of layers participating in the construction of this structure. Subdivided in this fashion, the structure can be represented as a consecutive stacking of the Y−Ge plane, a $[CoGa_4Ge_2]$ slab, and a puckered $[CoGa]_2$ layer.

The fragment of the Y−Ge plane viewed down the *c*-axis is shown in Figure 2B. The layer is defected, with the Ge atomic site being only 50% occupied. In the ideal YGe layer, the Y and Ge atoms are arranged in square-like manner, with Ge atoms being slightly off the plane of Y atoms. The distance between the Y and Ge in the plane is normal, 2.9641(6) Å; the Y−Y distance in the square net corresponds to the length of the unit cell, *a*. The $[CoGa_4Ge_2]$ slab, viewed approximately down the *c*-axis, is shown in Figure 2C. This type of layer has been previously observed in a number of ternary and quaternary intermetallic compounds such as Ce_2NiGa_{10},[20] Pr_3NiGa_{10},[21] Ce_4NiGa_{18},[22] Sm_2NiGa_{12},[8] $Sm_2Ni(Ni_xSi_{1-x})Al_4Si_6$,[1] $RE_2MGa_9Ge_2$,[7] and $Ce_2NiAl_{6-x}Ge_{4-y}$.[5] The layer consists of greatly compressed Ga_8 cubes, with the lengths of the cube sides being 2.590(3) and 2.9615(5) Å, that are condensed via face-sharing into a two-dimensional

(19) Sieve, B. Doctoral Dissertation Thesis, Michigan State University, 2002, Chapter 8.
(20) Yarmolyuk, Ya. P.; Grin', Yu. N.; Rozhdestvenskaya, I. V.; Usov, O. V.; Kuz'min, A. M.; Bruskov, V. A.; Gladyshevskii, E. I. *Sov. Phys. Crystallogr.* (translated from *Kristallografiya*) **1982**, *27*, 599.
(21) Grin', Yu. N.; Yarmolyuk, Ya. P.; Rozhdestvenskaia, I. V. *Sov. Phys. Crystallogr.* (translated from *Kristallografiya*) **1983**, *28* (4), 477.
(22) Grin', Yu. N.; Yarmolyuk, Ya. P.; Usov, O. V.; Kuz'min, A. M.; Bruskov, V. A. *Sov. Phys. Crystallogr.* (translated from *Kristallografiya*) **1983**, *28* (6), 710.

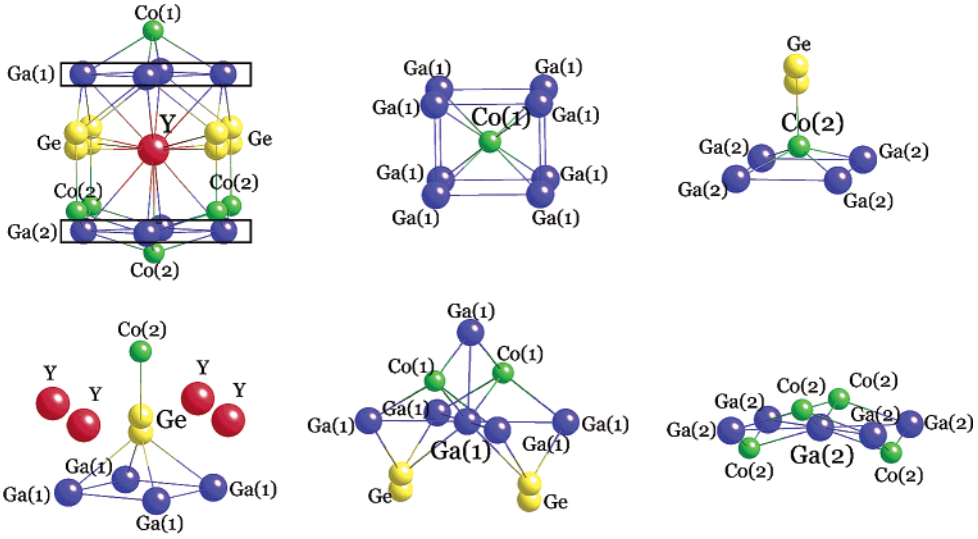

Figure 3. The local coordination of Y atoms within 3.5 Å, and Co, Ga, and Ge atoms within 3.0 Å. The Ge(1) and Ge(2) positions are depicted as one split Ge site.

Ga_4 framework. One half of the cubes in this framework are centered with Co(1) atoms, while the other half is vacant but capped with Ge atoms from above and below, see Figure 2C. The distance from the central Co(1) atom to the corners of the Ga(1) cube is 2.462(1) Å; the bond length between the capping Ge(2) and Ga(1) atoms is 2.677(3) Å. This slab is again defected, so that every second Ge(2) atom is missing.

Finally, the structure contains a $[CoGa]_2$ disordered puckered layer, in which Ga(2) atoms form a monatomic square net with a Ga(2)−Ga(2) distance of 2.9615(5) Å, see Figure 2D. The Co atoms are located above or below every Ga(2) square in a puckered manner. In this layer, every second Co(2) position is not occupied. In the structure of **1** the stacking sequence of the layers described above is *ABAC ABAC*, if YGe, $[CoGa]_2$, and $[CoGa_4Ge_2]$ slabs were denoted as *A*, *B*, and *C*, respectively.

The local coordination environments of the Y atoms within 3.5 Å and of the Co, Ga, and Ge atoms within 3.0 Å are presented in Figure 3. The Ge(1) and Ge(2) positions are regarded as one (split) Ge site. The Y atoms have four nearly in-plane contacts with Ge atoms; above and below this Y−Ge plane, the squares of $Ga(1)_4$ and $Ga(2)_4$ are located in staggered conformation to each other. The Co(1) capping the $Ge(1)_4$ square and five additional Co(2) atoms from the Ga(2)Co(2) puckered layer complete the 18-coordination sphere of Y atoms. The Co(1) is in the distorted cubic environment of eight Ga(1) atoms. The Co(2) local coordination is square-pyramidal with a square base made of Ga(2) atoms and an apex of Ge atom. Similarly, the Ge atom is in the center of a $Ga(1)_4Co(2)$ square pyramid. The Ga(1) atom is nine-coordinate, and it has a slightly distorted tetrahedral environment of two Co(1) and two Ge atoms (the Co(1)−Ga(1)−Ge angle is 109.12(4)°). The Ga(1) is additionally self-bonded to four atoms in the *ab*-plane (Ga(1)−Ga(1) = 2.9615(5) Å) and to one out-of-plane Ga(1) that caps the Co(1)−Co(1) edge of the tetrahedron. The Ga(2) is eight-coordinate, and its nearest coordination is formed by a severely distorted tetrahedron consisting of four Co(2) atoms

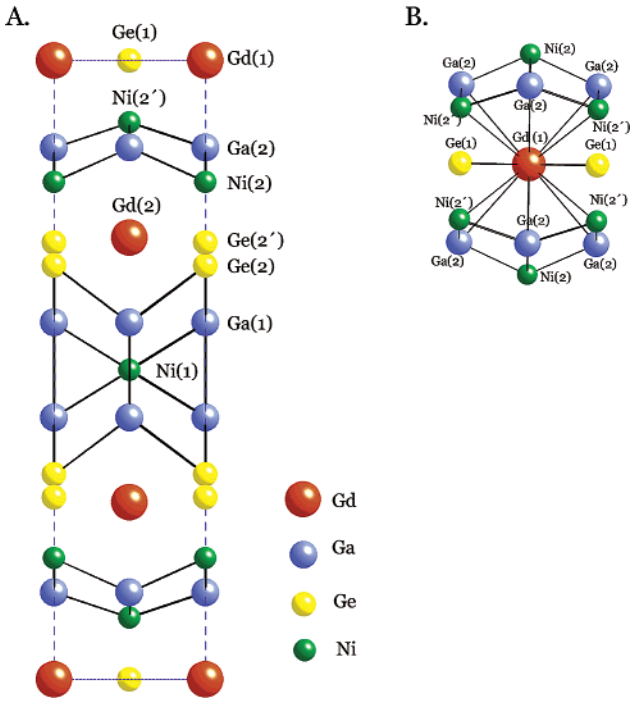

Figure 4. (A) The structure of $Gd_3NiGa_8Ge_3$ (**2**) viewed along the *b*-axis. (B) The local coordination of the Gd(1) atom. Only ordered atoms are shown; the Ge(2) and Ge(2′) positions are depicted as one split Ge(2) site.

(Co(2)−Ga(2) = 2.195(4) Å); the next four near-neighbors are four in-plane Ga(2) atoms bonded at 2.9615(5) Å.

Crystal Structure of 2. The crystal structure of $Gd_3Ni_3Ga_8Ge_3$ (**2**) is shown in Figure 4A and is reminiscent of that of $YCoGa_3Ge$ (**1**). Although the neutron structure refinement is not available for **2**, we are confident in assigning the Ga and Ge atoms analogously to **1**, considering the strong structural similarities of these two compounds. Using the same approach, the structure of **2** could be constructed of the similar building motifs as **1**; however, in the $Gd_3Ni_3Ga_8Ge_3$ the stacking sequence is different. Namely, the Gd−Ge (*A*) plane, a $[NiGa]_2$ (*B*) puckered layer, and $[NiGa_4Ge_2]$ (*C*) slab appear in the sequence *ABACABA ABACABA*.

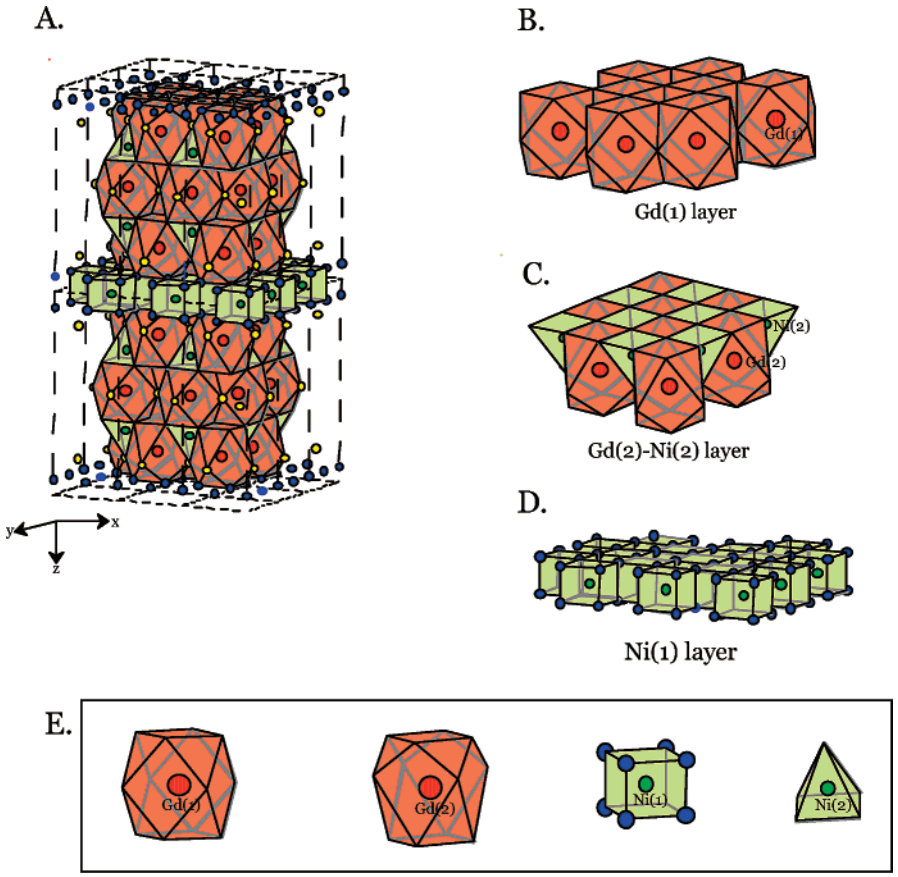

Figure 5. (A) The structure of $Gd_3NiGa_8Ge_3$ (**2**) in polyhedral representation. (B) The isolated layer of the Gd(1) cubo-octahedra. (C) The fragment of the Gd(2)−Ni(2) layer. (D) Distorted cubic layer of Ni(1). (E) Coordination polyhedra of Gd and Ni atoms in **2**.

The local environment of the ordered atoms in **2** is identical to those found in **1** with the exception of Gd(1), which is sandwiched between two $[NiGa]_2$ *B*-type layers and does not have a counterpart in **1**. The local coordination of the Gd(1) atom, remarkably, includes 22 atoms within a radius of 3.5 Å, see Figure 4B. The environment of the Gd(1) atom contains four Ge(1) atoms lying in a plane that includes Gd(1). Additionally, two fragments of the $[Ni(2')_4Ga(2)_4$-Ni(2)] puckered layer (related to each other by mirror symmetry) are located above and below the Gd(1)/Ge(1) plane.

It is useful to view the structure of **2** in polyhedral representation, see Figure 5A. The Gd(1) atoms are in ideal, and Gd(2) in distorted, cubo-octahedral environments of Ga and Ge atoms (within 3.2 Å). The Gd(1) cubo-octahedra are condensed into a 2D layer via sharing four out of their six square faces with each other, infinitely extending in the *ab*-plane, see Figure 5B. Likewise, the Gd(2) polyhedra share rhombic faces forming a 2D layer, see Figure 5C. In this Gd(2) layer, the pyramidal voids are occupied by Ni(2) atoms. The Ni(1) atoms are in a distorted cubic environment of Ga atoms. These cubes share edges to form a 2D Ni(1)−Ga(1) layer, as shown in Figure 5D. The Gd(1), Gd(2)−Ni(2), and Ni(1)−Ga(1) layers alternate along the *c*-axis and connected via face-sharing interactions between Gd and Ni polyhedra and via edge sharing between Gd(1) and Gd(2) cubo-octahedra. The coordination polyhedra of the Gd(1), Gd(2), Ni(1), and Ni(2) atoms are shown in Figure 5E.

Probing Long-Range Order with TEM and Electron Diffraction. The apparent disorder in the subcells of **1** and **2** motivated us to undertake a search for possible superstructure and long-range ordering with the help of electron diffraction. Because the nature of interaction of matter with electron beams is conceptually different from that of X-ray and neutron diffraction, and the interaction itself is much stronger, electron diffraction studies allow detecting weak satellite reflections often nearly invisible otherwise when using X-rays. Indeed, we find that the apparent disorder on the layers of REGe and $[MGa]_2$ is an artifact, and that these layers possess long-range order.

[001] Zone Axis of 1. The [001] zone axis photographs probe the structure of these materials in the *ab*-plane. The [001] zone axis SAED taken at room temperature on single crystals of **1** ($SmNiGa_3Ge$, $SmCoGa_3Ge$, and $GdCoGa_3Ge$) are shown in Figure 6A−C with the corresponding bright-field TEM images of the thin areas given below. The inspection of the thin electron-lucent area shows no irregularities in the way the crystal has developed. The cracks, if present, are random and most probably due to the stress imposed on the crystal during the TEM sample preparation. Luckily, the SAED patterns contained valuable information on the superstructure. In each of the three studied compounds, the SAED patterns feature both the subcell Bragg's reflections and the supercell reflections. While the subcell spots are intense, the supercell spots are generally weak. The systematic extinction of the strong subcell reflections satisfies

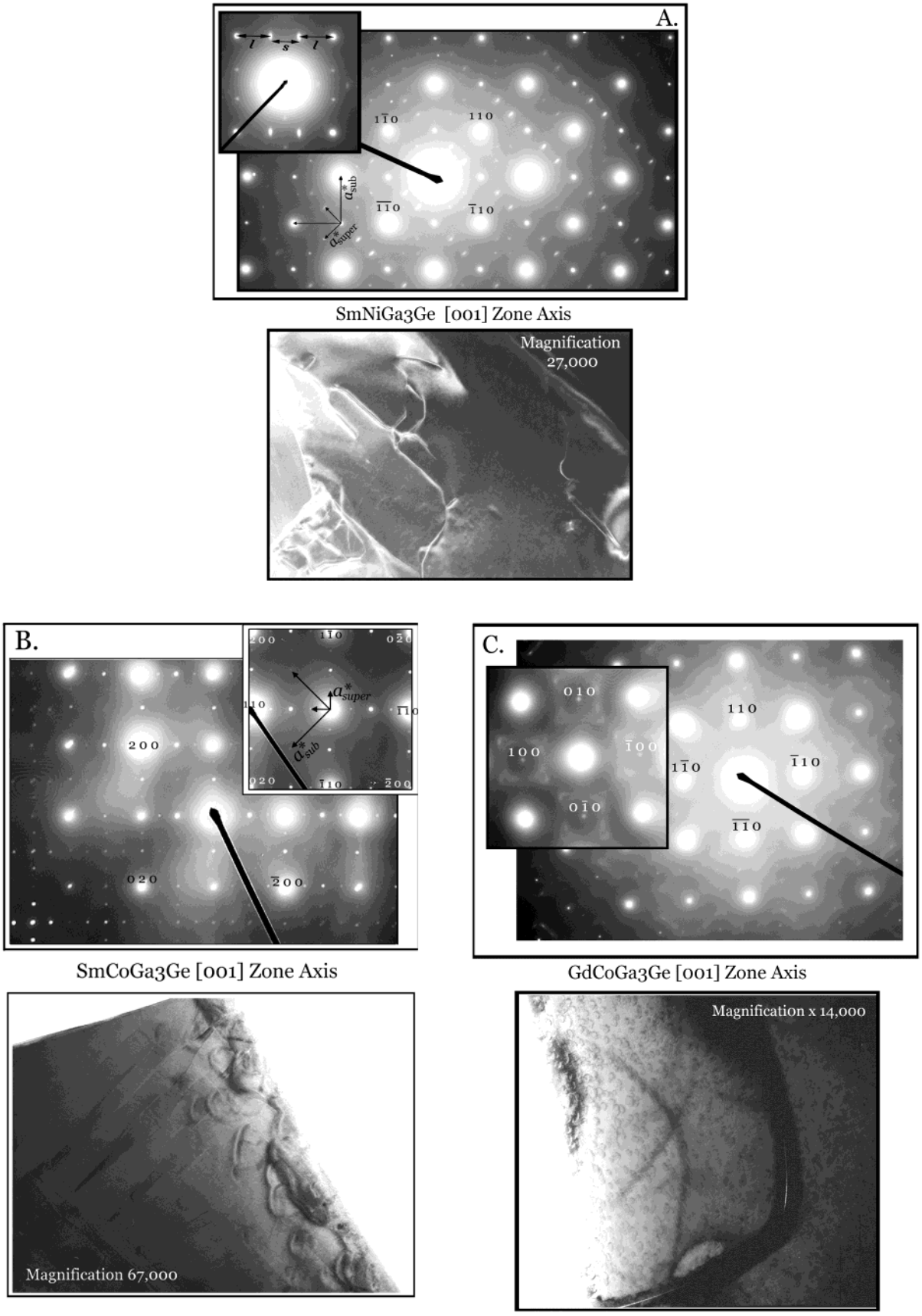

Figure 6. The [001] zone SAED pattern (top) and the TEM image (bottom) of **1**: (A) $GdCoGa_3Ge$, (B) $SmCoGa_3Ge$, and (C) $SmNiGa_3Ge$. No rotation calibration was performed.

the *I*-centering limiting condition for the *hk*0 set of reflections: $h + k = 2n$. The supercell reflections, on the other hand, do not display clear systematic absences and their positions are not commensurate with the underlying sublattice.

For example, in the SAED pattern of $SmNiGa_3Ge$, see Figure 6A, the spacings of the supercell reflections scale only approximately as $(1/3)a^*\sqrt{2}$, where a^* is a reciprocal subcell parameter. The magnified area of the reciprocal space of the $SmNiGa_3Ge$ is shown in the inset of Figure 6A. In order to describe the reciprocal supercell lattice, two unit vectors indicated by the letters "*l*" and "*s*" (which stand for "long" and "short" reciprocal lattice spacings) were used. These incommensurately spaced reflections propagate along both main axes of the reciprocal supercell (**a**′, **b**′); however, in one direction the supercell reflections seem to be stronger, suggesting the presence of an orthorhombic supercell and twinning.

Interestingly, the SAED pattern of the $SmCoGa_3Ge$ is different from that of the Ni analogue, signifying a different type of long-range order, see Figure 6B. In contrast to $SmNiGa_3Ge$, the $SmCoGa_3Ge$ does not exhibit incommensurate distances. In this case, the supercell reflections are equally intense in both directions and regularly spaced scaling as $(1/4)a^*\sqrt{2}$ with respect to the subcell a^*. Yet different diffraction behavior is seen for $GdCoGa_3Ge$. The [001] zone axis SAED pattern of $GdCoGa_3Ge$ stands out for its unusual diffraction pattern. Here, no discrete supercell spots could be easily recognized. Instead, diffuse scattering in the shape of the octagons and squares appears, see Figure 6C. The larger octagons are centered on the strong subcell reflections with $h + k = 2n$, while the smaller squares surround the subcell symmetry forbidden reflections with $h + k = 2n + 1$. Thus, using the tile of these two "unit cells", the 2D diffraction pattern could be constructed. It should be noted that the ED pattern featuring diffuse scattering has been repeatedly seen in a number of crystals of $GdCoGa_3Ge$.

[010] Zone Axis of 1. In order to probe the structure parallel to the layers, and examine the relative stacking of the *A*, *B*, and *C* layers mentioned above, diffraction experiments were performed with the electron beam directed parallel to the *b*-axis. In this fashion, we are observing the [010] zone. The [010] zone axis SAED pattern and corresponding thin area of $GdCoGa_3Ge$ are shown in Figure 7A and Figure 7B, respectively. Again, the diffraction pattern features both subcell reflections (strong) and supercell reflections (weak). The stronger subcell reflections conform to the limiting condition of *I*-centered cell for *h*0*l* set of reflections: $h + l = 2n$, consistent with *I*4/*mmm* space group of the substructure. No additional reflections corresponding to a supercell were observed along the reciprocal c^*-axis, which leads us to conclude that there is no superstructure along the c^*-axis. However, the supercell reflections with incommensurate periodicity of short and long spacings appear in the direction of the reciprocal a^*-axis. An interesting feature of these supercell reflections is their slightly elongated shape, along the c^*-direction. This could be attributed to stacking faults (not severe) of the *ab*-planes. A similar but more exacerbated situation was observed in the $RE_{0.67}M_2Ga_{5-x}Ge_x$[6] and $RE_{0.67}M_2Ga_{6-x}Ge_x$[6] families of compounds. For the latter two, the model was proposed, where the structure is considered to be constructed of the 2D building blocks fully ordered in the *ab*-plane, but stacked irregularly along the *c*-axis. Considering the similarities by which the disorder is expressed (streaking along the c^*-axis) in both $RE_{0.67}M_2Ga_{5+n-x}Ge_x$ ($n = 0, 1$)[6] and **1**, it is reasonable to adopt a similar model also in the case of **1**.

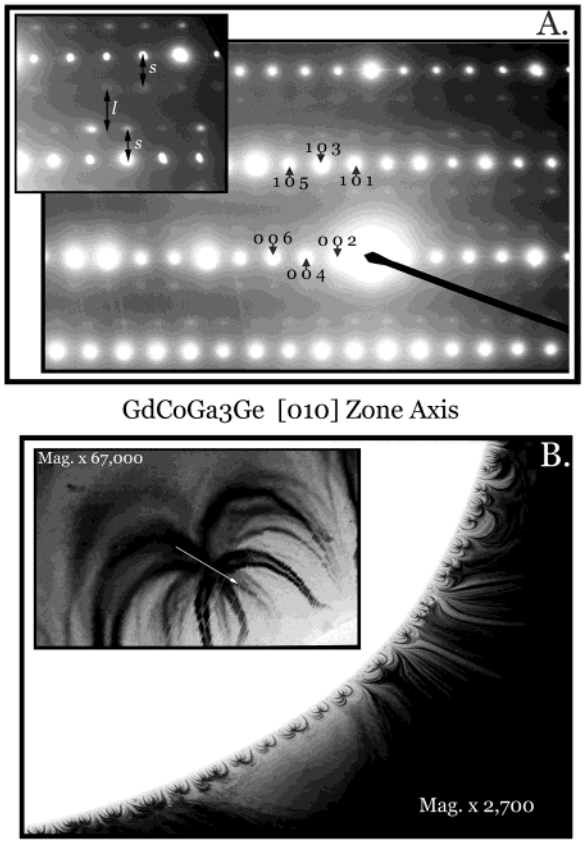

Figure 7. The [010] zone axis SAED pattern (A) and the TEM image (B) of $GdCoGa_3Ge$. No rotation calibration was performed.

The additional evidence that supports the stacking fault model might be found in examining the [010] zone TEM image, see Figure 7B. The thin area for [010] zone is noticeably different from that of [001] zone. Thus, the thin area around the edge is sliced by parallel lines (running at approximately 45° with respect to the tangent of the edge curvature) that could be associated with dislocation-type irregularities. It is rather improbable that the mentioned irregularities can be caused by the TEM sample preparation, as exactly the same conditions were applied to prepare both [001] and [010] zone axis samples. Nevertheless, further high-resolution TEM studies are necessary to confirm the stacking fault origin of the disorder.

To summarize, the superstructures found in **1** take place in the *ab*-plane only, whereas the direction of the *c*-axis is not modulated. The in-plane modulation varies from analogue to analogue and reaches up to 8-fold supercell in volume ($SmCoGa_3Ge$). In some instances the period of modulation scales incommensurately with underlying sublattice. The investigation of incommensuration observed in a number of

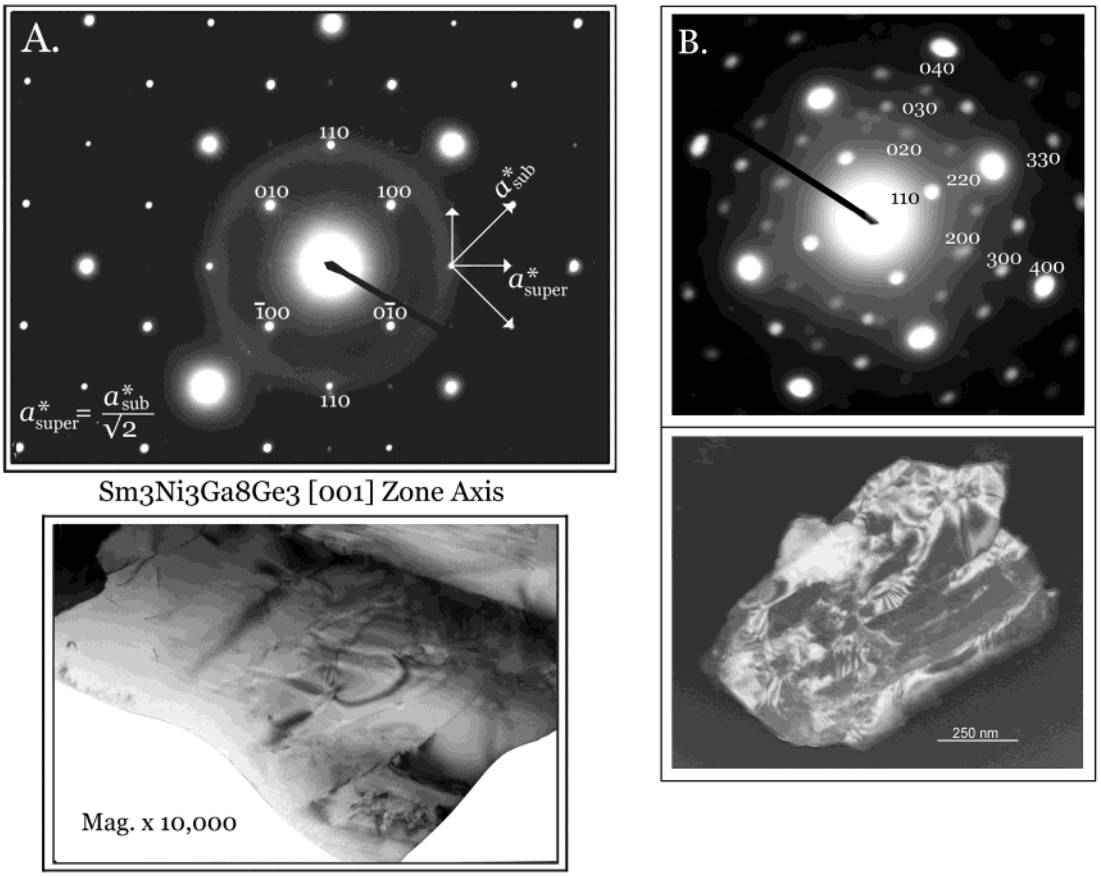

Figure 8. The [001] zone axis of **2**: SAED pattern and the TEM image of (A) $Sm_3Ni_3Ga_8Ge_3$ and (B) $Gd_3Ni_3Ga_8Ge_3$. No rotation calibration was performed.

Co analogues of **1** using a superspace approach is currently in progress.[23] It is yet unclear what causes the variety of complex ordering in the *ab*-plane to occur in different analogues of **1**. One possibility is that the occupancy of the transition metal site may vary slightly from compound to compound. However, a size effect has to be ruled out, as different superstructures were obtained for the analogues with the elements of similar radii (compare $SmMGa_3Ge$ (M = Ni and Co) and $RECoGa_3Ge$ (RE = Sm and Gd)). On the other hand a variety of superstructures reminiscent of the type observed in the compounds described here have been found to be pervasive in many polytelluride compounds that contain square nets of Te atoms. The origin of those superstructures is energy-lowering, displacive modulations in the Te square nets the nature of which depends primarily on the average charge on Te and secondarily on the RE element.[24] It is possible that the effect extends to square nets of other elements such as Ga. Further studies are necessary to examine the superstructures in details and the reasons that give rise to them.

[001] Zone Axis of 2. The [001] zonal axis shows crystallographic *ab*-plane. The [001] zone axis SAED pattern and the thin area of $Sm_3Ni_3Ga_8Ge_3$ and $Gd_3Ni_3Ga_8Ge_3$ (**2**) are presented in Figure 8. Similarly to **1**, the [001] zone electron diffraction patterns of **2** contain the information on the supercell. The SAED pattern of the Sm analogue of **2** is given in Figure 8A. The subcell reflections reveal no systematic absences, in accord with a primitive Bravais lattice. In addition to the subcell reflections, the electron diffraction pattern features very weak supercell reflections. The supercell parameters in the *ab*-plane were found to be $(1/2)a^*\sqrt{2} \times (1/2)a^*\sqrt{2}$. Likewise, the SAED pattern obtained for Gd analogue, see Figure 8B, also exhibits a $(1/2)a^*\sqrt{2} \times (1/2)a^*\sqrt{2}$ supercell. Thus, in contrast to **1**, consistent supercell parameters were obtained for Gd and Sm analogues of **2**. Assuming no modulation takes place along the *c*-axis (as it is in case of **1**), the supercell of **2** is 2-fold ($a\sqrt{2} \times a\sqrt{2}$). Because the supercell reflections were extremely weak, no X-ray data supporting the supercell could be obtained for either **1** or **2** compounds.

Magnetic Properties. Magnetism of 1 ($TbNiGa_3Ge$, $GdCoGa_3Ge$ and $YCoGa_3Ge$). (a) Tb Analogue. The magnetic properties were studied for three analogues of **1** (RE = Tb, Gd, and Y). The temperature dependence of susceptibility of a polycrystalline sample of the $TbNiGa_3Ge$ calculated per mole of Tb is shown in Figure 9A. The susceptibility shows an antiferromagnetic maximum at ~5 K; below that temperature the zero-field cooled (ZFC) and field cooled (FC) parts of susceptibility diverge, see inset in Figure 9A. Above 30 K the reciprocal susceptibility increases linearly with temperature, indicating Curie−Weiss behavior, see Figure 9B. The effective magnetic moment (μ_{eff})

(23) Zhuravleva, M. A.; Evain, M.; Petricek, V.; Kanatzidis, M. G. Manuscript in preparation.
(24) Kanatzidis, M. G.; Patschke, R. *Phys. Chem. Chem. Phys.* **2002**, *4*, 3266.

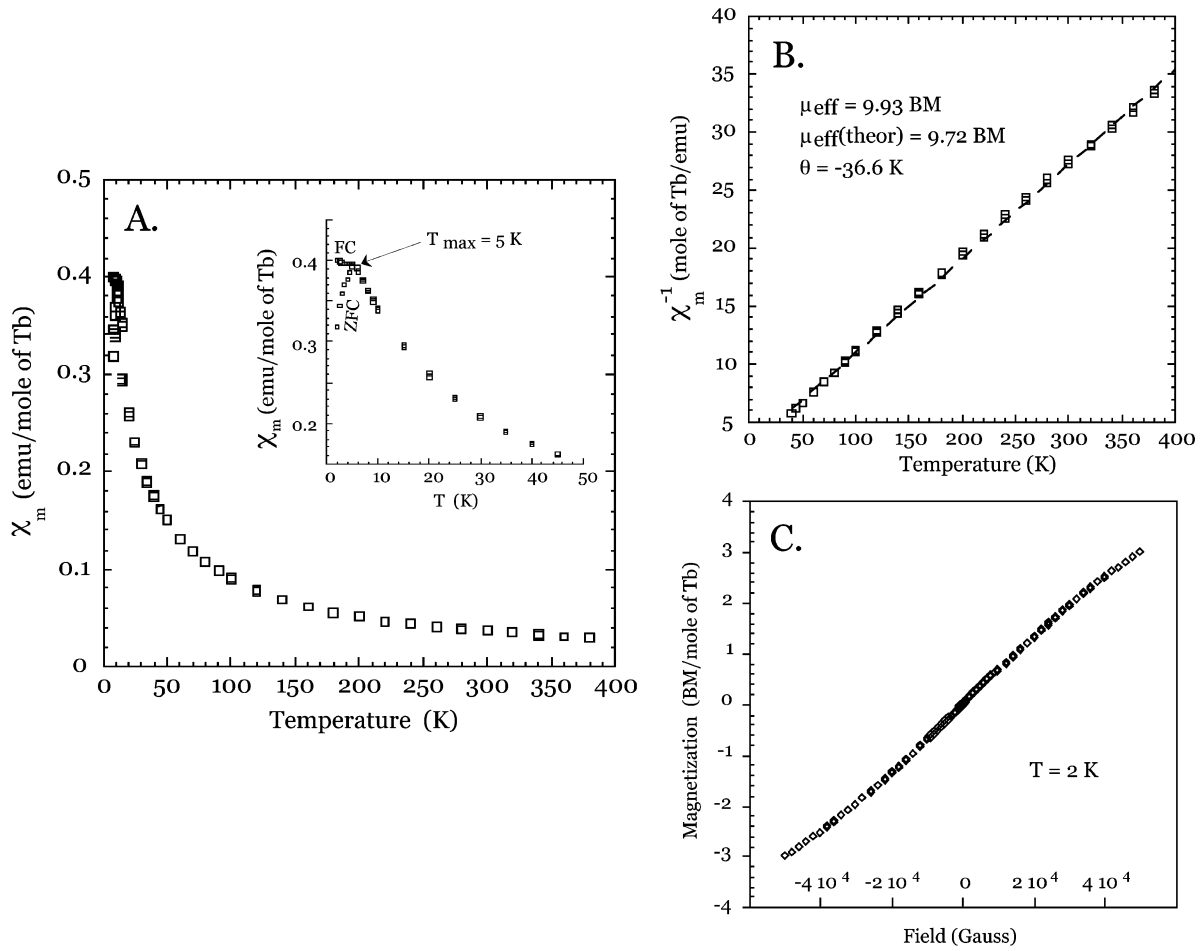

Figure 9. The magnetization data for the $TbNiGa_3Ge$ polycrystalline sample. (A) Temperature dependence of molar magnetic susceptibility. Inset: Low-temperature region of magnetic susceptibility. (B) Inverse susceptibility. (C) The molar magnetization in fields up to ±5 T.

calculated from the linear part of the plot is 9.93 μ_B, in agreement with the free-ion value for Tb^{3+} (9.72 μ_B). The Ni atoms accordingly do not have a localized magnetic moment, i.e., their contribution to the susceptibility is diamagnetic. The Weiss constant is negative, $\Theta = -36.6$ K, in accord with proposed antiferromagnetic ordering. The magnetization in fields up to ±5 T is nearly linear and shows no saturation, with a maximal moment of 3 μ_B developed in the field 5 T that corresponds to only 30% of the full saturation value, see Figure 9C.

(b) Gd Analogue. The magnetic properties of the $GdCoGa_3Ge$ analogue were studied in both polycrystalline (isotropic) and single crystal (anisotropic) type measurements. The molar susceptibility data vs temperature is plotted in Figure 10A. For the Gd analogue, the T_{max} occurs at higher temperature compared to the Tb analogue, at ~15 K, as shown in the inset in Figure 10A. At the temperature 50 K and higher, the inverse magnetic susceptibility obeys Curie–Weiss law, see Figure 10B, with the average $\mu_{eff} = 8.15$ μ_B close to the free-ion value for Gd^{3+} (7.94 μ_B). The exact values for μ_{eff} and Θ for different orientations are $\mu^{\parallel c} = 8.42$ μ_B, $\mu^{\perp c} = 8.43$ μ_B, $\mu^{iso} = 7.62$ μ_B, $\Theta^{\parallel c} = -56$ K, $\Theta^{\perp c} = -54$ K, and $\Theta^{iso} = -47$ K. The negative sign of the Weiss constants is again in favor of the antiferromagnetic moments ordering on the Gd atoms. The subsequent determination of the Néel temperature from the set of isofield plots of χ_m vs T yielded $T_N = 15$ K.

The field dependence of magnetization for all orientations is presented in Figure 10C. The maximum moment developed in the field of 5 T does not exceed 1 μ_B, which is only 14% of the full saturation value. From both temperature- and field-dependence measurements, it is evident that the relative crystal-to-field orientation does not produce any impact on magnetization and susceptibility. Thus, the effect of crystal field in $GdCoGa_3Ge$ is obviously negligible. Such isotropic behavior of magnetization is consistent with S-state of the Gd^{3+} atoms and has been previously observed in a number of Gd-containing intermetallic compounds including $Gd_{0.67}Ni_2Ga_{5-x}Ge_x$[6] and Gd_3Ga_9Ge,[25] as well as in pure Gd metal.[26]

(c) Y Analogue. The effective magnetic moments obtained for the analogues of **1** with Gd and Tb indicate that the magnetic moments are carried solely by the rare-earth ions, while the transition metals are in diamagnetic state. However, in order to reconfirm the nonmagnetic nature of the transition metal atoms (Ni and Co), magnetic measurements were

(25) Zhuravleva, M. A.; Kanatzidis, M. G. *J. Solid State Chem.* **2003**, *173*, 280.
(26) Rhyne, J. J. In *Magnetic Properties of Rare Earth Metals*; Elliot, R. J., Ed.; Plenum Press: London and New York, 1972.

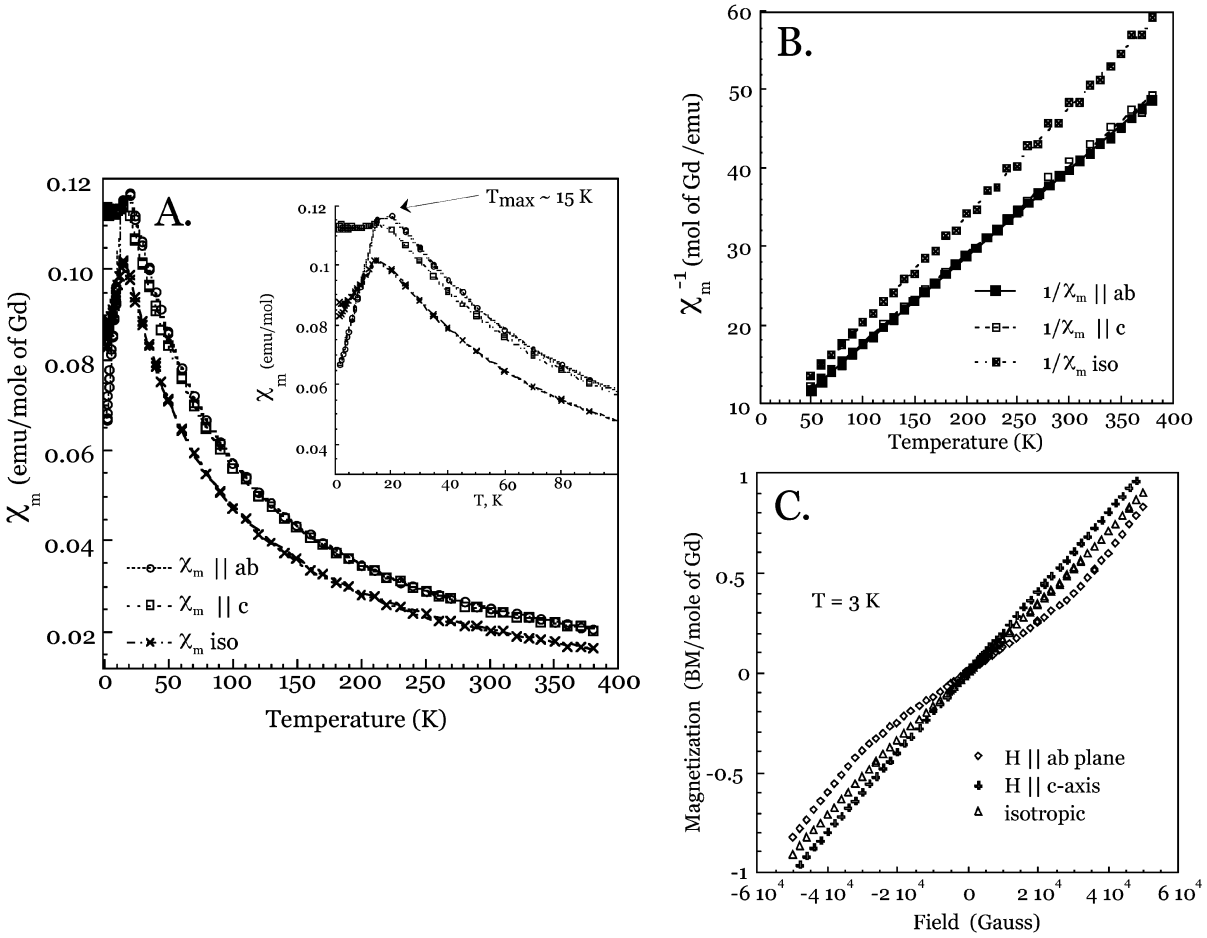

Figure 10. (A) Temperature dependence of molar magnetic susceptibility and (B) inverse susceptibility of $GdCoGa_3Ge$ single crystal oriented with [100] axis parallel, perpendicular to the external magnetic field (H_{ex}) and isotropic. Inset: Magnetic susceptibility in the proximity of an antiferromagnetic transition temperature. (C) The molar magnetization in fields up to ±5 T.

performed using the Y analogues, since Y^{3+} is diamagnetic. As a result, the susceptibility of $YCoGa_3Ge$ was determined to be very low (0.6×10^{-3} emu/mol or 0.6×10^{-9} m^3/mol) and nearly temperature independent, which is characteristic of Pauli paramagnetism. Thus, in **1** the magnetic moments indeed originate only from rare-earth atoms, whereas the Ni and Co atoms are in diamagnetic states. This situation is now a recurring theme in this type of intermetallic chemistry, since similar diamagnetic behavior of the transition metal atoms was also observed in Sm_2NiGa_{12},[8] $RE_{0.67}Ni_2Ga_{5+n-x}Ge_x$,[6] $RENiSi_3$,[27] $RENiAl_4Ge_2$,[3] $Sm_2Ni(Ni_xSi_{1-x})Al_4Si_6$,[1] $RE_4FeGa_{12-x}Ge_x$,[28] and many other related intermetallic compounds.

Magnetism of 2: $Gd_3Ni_3Ga_8Ge_3$. The temperature dependence of the susceptibility of a single crystal of **2** ($Gd_3Ni_3Ga_8Ge_3$) is presented in Figure 11A. The maximum of the magnetic susceptibility occurs at ~10 K. Slight variation of the ZFC−FC parts is observed below that temperature. In Figure 11B the inverse magnetic susceptibility (χ_m^{-1}) is plotted against the temperature. The linear increase in χ_m^{-1} with temperature and nonzero intercept with temperature axis indicate Curie−Weiss behavior; the Weiss constant and the effective magnetic moment were determined to be −40.7 K and 8.24 μ_B, respectively. Both the sign and the maximum on χ_m indicate the antiferromagnetic ordering below T_{max}.The Néel temperature $T_N = 10$ K was determined from the set of the isofield $\chi_m - T$ plot by extrapolating the maximal temperature to the zero field. The μ_{eff} found for $Gd_3Ni_3Ga_8Ge_3$ is in agreement with the free-ion value for Gd^{3+} ion. Similarly to **1**, the Ni atoms in **2** are in nonmagnetic state. The magnetization increases linearly with the applied magnetic field, reaching the value of only 1.5 μ_B in fields of 5 T, see Figure 11C.

Concluding Remarks

In liquid Ga the elements RE, M, and Ge with RE:M ≥ 1 react readily to give well-grown crystals of two different families of new quaternary compounds $REMGa_3Ge$ (M = Ni, Co) and $RE_3Ni_3Ga_8Ge_3$. The flux method proves to be an excellent tool for discovering new quaternary intermetallic compounds with complex stoichiometries. In compounds containing Ga and Ge (just as for those containing Al and Si), it is often difficult to assign with a high degree of confidence the corresponding sites, requiring neutron diffraction analysis in some representative cases. The single-crystal neutron diffraction performed on $YCoGa_3Ge$ shows that Ge is situated on the 4*e* site, while Ga atoms occupy 4*d*

(27) Chen, X. Z.; Larson, P.; Sportouch, S.; Brazis, P.; Mahanti, S. D.; Kannewurf, C. R.; Kanatzidis, M. G. *Chem. Mater.* **1999**, *11*, 75.
(28) Zhuravleva, M. A.; Wang, X.; Schultz, A. J.; Bakas, T.; Kanatzidis, M. G. *Inorg. Chem.* **2002**, *41*, 6056.

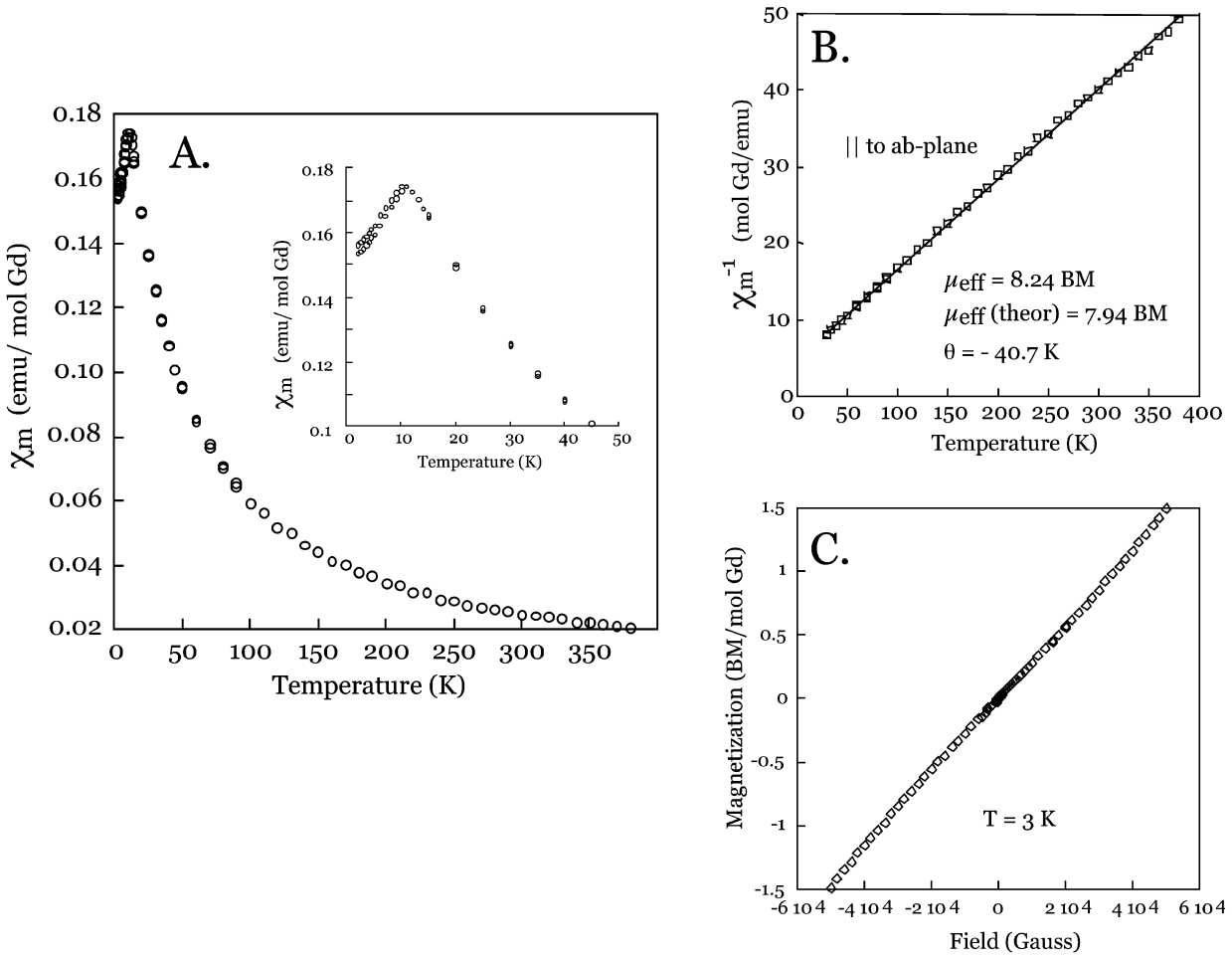

Figure 11. (A) Temperature dependence of molar magnetic susceptibility and (B) inverse susceptibility of $Gd_3Ni_3Ga_8Ge_3$ single crystal. Inset: Magnetic susceptibility in the proximity of an antiferromagnetic transition temperature. (C) The molar magnetization in fields up to ±5 T.

and 8*g* crystallographic sites. The structures contain square nets of Ga atoms arranged in layers. Both the X-ray and neutron diffraction structural refinements give evidence of a "disorder" taking place in the REGe and $[MGa]_2$ slabs, which actually is an artifact of the small unit cell. Investigations performed with electron diffraction indicate that in $REMGa_3Ge$ a complex long-range ordering occurs in the *ab*-plane, that varies in nature with the RE element. Various types of superstructures, up to 8-fold in volume ($2a\sqrt{2} \times 2a\sqrt{2}$), were found for the analogues of $REMGa_3Ge$. For the $RE_3Ni_3Ga_8Ge_3$, the superstructure also takes place in the *ab*-plane, and was determined to be 2-fold ($a\sqrt{2} \times a\sqrt{2}$). The origin of the long-range ordering is believed to be displacive modulations occurring in the Ga square nets.[23] This phenomenon is intriguing and deserves further investigations. The magnetic moments in these materials are localized on the RE atoms, while the transition metal atoms are in nonmagnetic state. Antiferromagnetic ordering transitions are observed in $TbNiGa_3Ge$, $Gd_3Ni_3Ga_8Ge_3$, and $GdCoGa_3Ge$ at Néel temperatures of 5, 10, and 15 K, respectively. The Gd analogues of $RECoGa_3Ge$ and $RE_3Ni_3Ga_8Ge_3$ show no magnetic anisotropy in accord with S-ground state of Gd^{3+} ion.

Acknowledgment. Financial support from the Department of Energy (Grant DE-FG02-99ER45793) is gratefully acknowledged. This work made use of the SEM/TEM/EDS facilities of the Center of Advanced Microscopy at Michigan State University. We are indebted to Prof. M. A. Crimp of the Department of Chemical Engineering and Material Science at Michigan State University for providing the electropolishing unit and for fruitful discussions. The work at Argonne National Laboratory was supported by the U.S. Department of Energy, Basic Energy Sciences-Materials Sciences, under Contract No. W-31-109-ENG-38. M.G.K. thanks the Guggenheim Foundation for a fellowship.

Supporting Information Available: Two X-ray (for compounds **1** and **2**) and one neutron (for compound **1**) crystallographic files, in CIF format. This material is available free of charge via the Internet at http://pubs.acs.org.

IC0341892